Tikrit Journal of Engineering Sciences (2025); 32(3): 2255
DOI: http://doi.org/10.25130/tjes.32.3.32

IRAQI Academic Scientific Journals

ISSN: 1813-162X (Print); 2312-7589 (Online)
Tikrit Journal of Engineering Sciences
available online at: http://www.tj-es.com

TJES Tikrit Journal of Engineering Sciences

Sliding Mode Control with Multilevel Inverter for PMSM Motor

Asaad F. Nashee [a]*, Mohammed A. H. Ali [b], Naif Mohammad AL-Shammary [c], Atheer L. Salih [d]

a Department of Information and Communications Technology, Institute of Technology Middle Technical University, Iraq.
b Department of Mechanical Engineering, University of Malaya, Malaysia.
c Saudi Chevron Company Engineering Department, Partition Zone (PZ) - Kingdom of Saudi, Arabia.
d Electrical Department, Engineering, Baden-Wuerttemberg Cooperative State University, Ravensburg, Germany.

Keywords:
Multilevel inverter; PMSM motor; Sliding mode control; SVPWM modulation; Wavelet transform.

Highlights:

- Sliding Mode control based Multilevel inverter.
- Wavelet transform for feature extraction.
- PMSM motor with space vector pulse width modulation (SVPWM).

ARTICLE INFO
Article history:

Received	06 July 2024
Received in revised form	12 Aug. 2024
Accepted	19 Aug. 2024
Final Proofreading	20 Aug. 2025
Available online	28 Aug. 2025

Citation: Nashee AF, Ali MAH, AL-Shammary NM, Salih AL. **Sliding Mode Control with Multilevel Inverter for PMSM Motor**. *Tikrit Journal of Engineering Sciences* 2025; **32**(3): 2255.
http://doi.org/10.25130/tjes.32.3.32

Corresponding author:
Asaad F. Nashee
Department of Information and Communications Technology, Institute of Technology Middle Technical University, Iraq.

Abstract: This paper introduces a permanent magnet synchronous motor (PMSM) with a sliding mode control (SMC)-based wavelet transform (WT). The PMSM motor is vulnerable to variations in the motor parameters and external disturbances, which may deteriorate steady-state performance. The proposed control system was tested using a 3-φ PMSM motor with 5 kW, 1000RPM, and a 3-φ multilevel inverter. The results showed that the motor can reach the estimated speed with good tracking to the value set at a frequency varying from [400, 1000, and 200] RPM. The system uses the Daubechies wavelets (db) for feature extraction due to their localization in both the time and frequency domains. A multilevel inverter with the space vector pulse width modulation (SVPWM) modulation algorithm was used to decrease the total harmonic distortion (THD) of the system to less than 2.5%, with WT residuals almost zero, with 100% decomposition and reconstruction. MATLAB 2020a was used for mathematical modeling and simulation of the proposed algorithm. The simulation results ensured smooth operation in all regions for the PMSM motor's speed and torque.

التحكم في وضع الانزلاق مع عاكس متعدد المستويات للمحرك المتزامن ذو المغناطيس الدائم

اسعد فنجان ناشي[١]، محمد عبدو هاشم علي[٢]، نايف محمد الشمري[٣]، اثير لؤي صالح[٤]

[١] قسم تكنولوجيا الاتصالات والمعلومات/ معهد التكنولوجيا / الجامعة التقنية الوسطى/ العراق.

[٢] قسم الهندسة الميكانيكية/ جامعة مالايا/ ماليزيا

[٣] قسم الهندسة/ شركة شيفرون/ المملكة العربية السعودية.

[٤] قسم الهندسة الكهربائية /جامعة ولاية بادن /المانيا.

الخلاصة

يقدم هذا البحث المحرك المتزامن ذو المغناطيس الدائم الذي يعتمد على التحكم في الوضع المنزلق مع محول الموجات (WT). هذا المحرك عرضة للتغيرات في معلمات المحرك والاضطراب الخارجي، مما قد يؤدي إلى تدهور أداء الحالة المستقرة. محرك 5 kW ، ١٠٠٠ دورة في الدقيقة مع عاكس متعدد المستويات ثلاثي الطور استخدم في هذا البحث لاختبار نظام التحكم المقترح. اظهرت النتائج أن المحرك يحقق السرعة المقدرة مع سرعة تتبع جيدة حسب القيمة المحددة من خلال تغير السرعات من [٤٠٠-١٠٠٠-٢٠٠] دورة في الدقيقة. تم استخدام مويجات Daubechies (db) لاستخراج ميزات النظام بسبب توطينها في مجال الوقت والتردد. إن استخدام عاكس متعدد المستويات مع خوارزمية تعديل عرض نبضة متجه الفضاء (SVPWM) يقلل من التشوه التوافقي الكلي للنظام الى اقل من 2.5% مع نسبة صفر تقريبا للمتبقي من عملية فصل واعادة تشكيل محول المويجات التي كانت بنسبة ١٠٠٪. تم استخدام MATLAB 2020 a في النمذجة الرياضيه والمحاكاة للخوارزمية المقترحة. نتائج المحاكاة تؤكد التشغيل السلس في جميع المناطق من حيث سرعة وعزم دوران المحرك المتزامن ذو المغناطيس الدائم.

الكلمات الدالة: عاكس متعدد المستويات، المحرك المتزامن ذو المغناطيس الدائم، التحكم في وضع الانزلاق، تعديل عرض نبضة متجه الفضاء، تحويل المويجات.

1.INTRODUCTION

Industrial applications extensively use Permanent Magnet Synchronous Motors (PMSM) due to their compact size, excellent speed control, and high efficiency. The load torque and rotational inertia will, however, fluctuate often during PMSM operation, which will impact the control system's efficiency. Increasing the system's anti-interference capabilities and strengthening the durability of parameter changes are essential for achieving optimal performance. Researchers in this instance employ a variety of cutting-edge theories to enhance the performance of the PMSM control system. Several popular techniques include intelligent control, sliding mode control (SMC), adaptive control, robust control, and so on. Due to their strong robustness and ease of implementation, PMSM control systems have been widely studied and applied, including SMC among these methods [1]. Electric vehicles and industrial applications have shown a great deal of interest in multilevel inverters (MLIs) [2]. This interest stems from the fact that 2-level inverters frequently struggle to match the grid voltage ranges due to semiconductor blocking voltages. Consequently, MLIs have become the standard option for grid interfacing. The sliding mode control is a simple, effective control method that works based on feedback from the system's state variables [3]. In such a controller, the inverter has a phase-modulated carrier (PM-phase modulation) to reduce total harmonic distortion (THD) in torque and current and to reduce the common-mode voltages to achieve the best possible result. The main objective of SMC is to choose the sliding function and its derivative to simplify higher-order systems. The outstanding advantages of SMC are fast response time, no overshoot, no oscillation, zero speed setting error, and a high nominal quality controller [4]. The PMSM motor drives' signal characteristics are extracted via wavelet analysis. In the field of high-power and medium-voltage energy regulation, multilevel inverters have become an essential substitute technology. Semiconductor power devices are frequently utilized due to their lower blocking voltage requirements, lower output voltage THD %, and lessened stress on the insulation. In industrial applications, the semiconductor power device is the most brittle part [5]. The proportional-integral (PI) controller finds it challenging to achieve good control results in both rapidity and immunity [6, 7]. Sliding mode control (SMC), one of many nonlinear control techniques proposed to improve PMSM performance, has attracted attention due to its robustness and quick response times. Three main steps are involved in designing the SMC system: selecting the sliding mode surface, formulating the reaching law, and determining the control rate [8]. A standard AC-DC-AC three-level electrical drive arrangement achieves higher power and reduced harmonics [9]. Three-level neutral-point-clamped (3LNPC) inverters are a type of multilevel inverter that keeps the unity power factor, stabilizes the DC link voltage, and allows sinusoidal input current. There are four main types of multilevel inverters: H-bridge multilevel inverters, capacitor-clamped or flying-capacitor multilevel inverters, and diode-clamped or neutral-point-clamped multilevel inverters. This study proposes a non-singular continuous sliding mode control method with a wavelet to enhance the position tracking performance and robustness of the PMSM servo system, while also addressing the non-singularity of SMC control. First, the algorithm replaces the switching function with a continuous function to mitigate its

discontinuity. It then adjusts the SMC parameters online and in real-time, extracting signals using a wavelet-based control to minimize system chattering due to improper parameter settings. Second, the current loop utilizes Direct-quadrature(dq) voltage quantities to guarantee the current condition upon motor startup and counteract any fluctuations resulting from changes in internal parameters. Also, the advantages of both WT and SMC are that they can adjust the duty cycle of the inverter to satisfy optimal conditions of operation in terms of speed and torque without producing steady state error. The approximate nonlinear WT and fast convergence ability of the WT system are used to approximate the system uncertainties integrated with the SMC performance, such as lower switching gain. Finally, the PMSM position control system tests this technology using continuous SMC with multilevel inverters as the controller. To evaluate the control approach, MATLAB/Simulink R2020a simulations are run. This paper's structure is as follows: Section II describes the mathematical model for PMSM. Section III introduces the sliding mode control technique. Section IV presents the proposed multilevel inverter. Section V describes the wavelet-based feature extraction process. Sections VI and VII present the simulation results and conclusions, respectively.

2.PMSM MATHEMATICAL MODEL

Figure 1 depicts the PMSM motor with a single pole pair on the rotor.

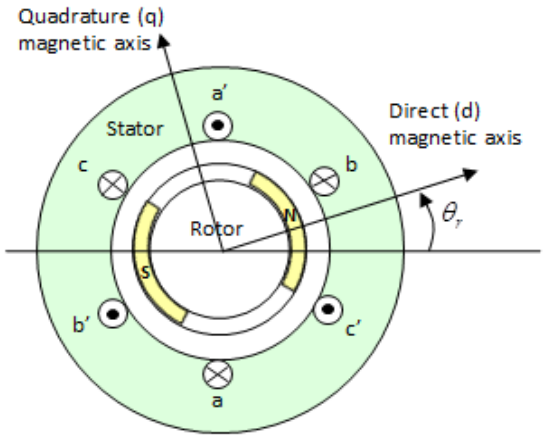

Fig. 1 The PMSM Motor Architecture Features a Single Rotor Pole Pair.

The cross-coupling, angular speed, and current on the d and q axes make the PMSM's dynamic model nonlinear. The aforementioned PMSM model was linearized by creating additional variables, as explained in [10]. If the magnetic field is considered as symmetric in the motor, the PMSM can then be simplified with a model of a third-order state space model, as in Eq. (1) [11]. where $J, D, \theta, L, and\ \psi$ represent the rotor and load inertia, damping coefficient, rotor angular position, load torque, and flux amplitude caused by the rotor's permanent magnets in the stator phases. The specifications of the PMSM motor used in the present work are shown in Fig. 2. Figure 3 displays the electrical portion of the PMSM that Simulink implemented.

$$A = \begin{bmatrix} -\frac{R}{L} & -\frac{\psi P}{L} & 0 \\ \frac{1.5\psi P}{J} & \frac{-D}{J} & 0 \\ 0 & 1 & 0 \end{bmatrix}, B = \begin{bmatrix} 1/L \\ 0 \\ 0 \end{bmatrix}, C = [0\ 1\ 0] \quad (1)$$

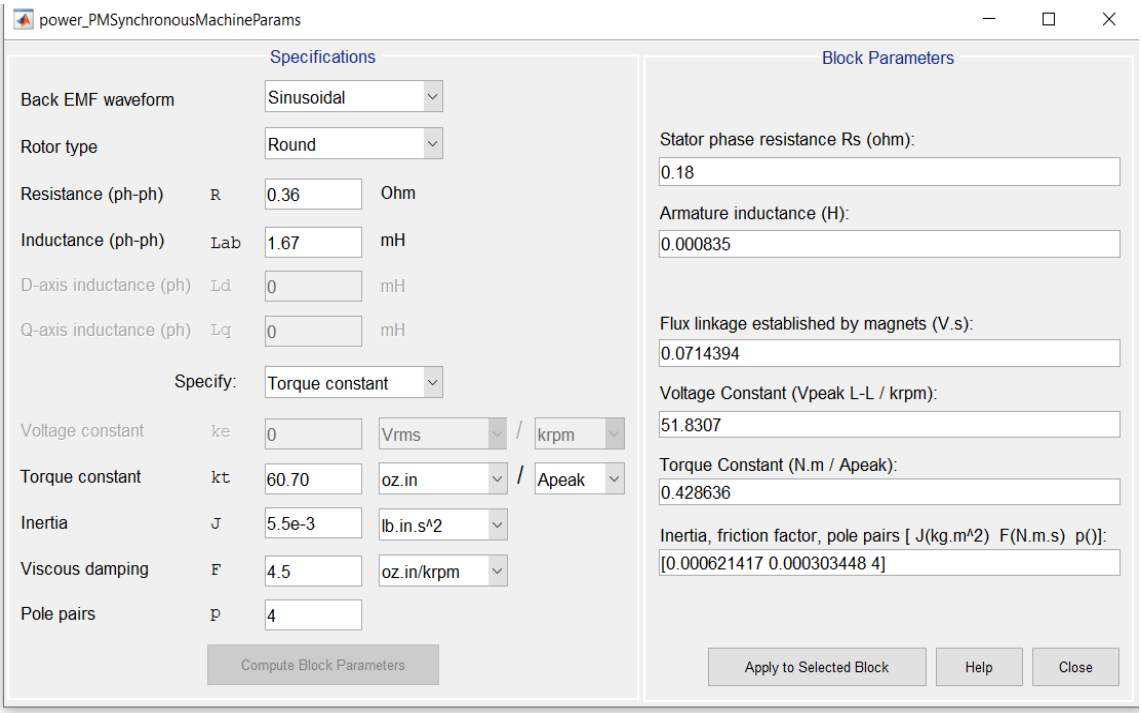

Fig. 2 PMSM Motor Specifications.

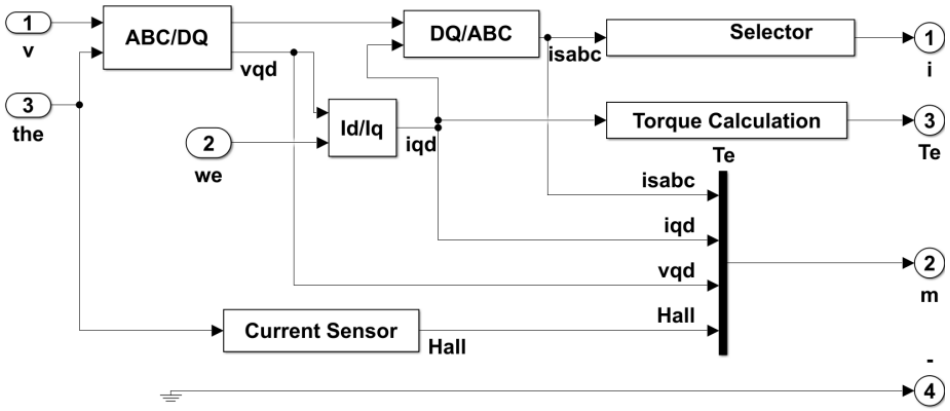

Fig. 3 The PMSM Motor's Electrical Component.

The mechanical part of the PMSM model is computed depending on the motor torque, as in Eq. (2).

$$T_e = \frac{3n_p}{2K^2}((L_{sd} - L_{sq})i_{sd}i_{sq} + i_{sq}\psi_m \quad (2)$$

The expressions for stator flux linkages in the three-phase model are provided in Eqs. (3-5):

For Phase a:

$$\Psi_a = L_{aa}i_a + L_{ab}i_b + L_{ac}i_c + \Psi_m \cos(\phi_r) \quad (3)$$

For Phase b:

$$\Psi_b = L_{ba}i_a + L_{bb}i_b + L_{bc}i_c + \Psi_m \cos\left(\phi_r - \tfrac{2\pi}{3}\right) \quad (4)$$

For Phase c:

$$\Psi_c = L_{ca}i_a + L_{cb}i_b + L_{cc}i_c + \Psi_m \cos\left(\phi_r + \tfrac{2\pi}{3}\right) \quad (5)$$

where *Laa, Lbb, and Lcc* are the self-inductances of the stator a-phase, b-phase, and c-phase, respectively, and Ψm is the flux linkage established by the permanent magnet. Equations (6–8) provide an expression for the three-phase stator voltages in the coupled circuit.

$$u_a = R_a i_a + \frac{d\psi_a}{dt} \quad (6)$$

$$u_b = R_b i_b + \frac{d\psi_b}{dt} \quad (7)$$

$$u_c = R_c i_c + \frac{d\psi_c}{dt} \quad (8)$$

The voltage equations in d-q rotating coordinates are expressed by Eqs. (9) and (10):

$$u_{sd} = R_s i_{sd} + L_{sd}\frac{di_{sd}}{dt} - \omega_r L_{sq} i_{sq} \quad (9)$$

$$u_{sq} = R_s i_{sq} + L_{sq}\frac{di_{sq}}{dt} + \omega_r L_{sq} i_{sq} + \omega_r \psi_m \quad (10)$$

Figure 4 shows the modeling of the mechanical element of the PMSM motor using discontinuous forward Euler trapezoidal integration of machine equations in the stationary reference frame.

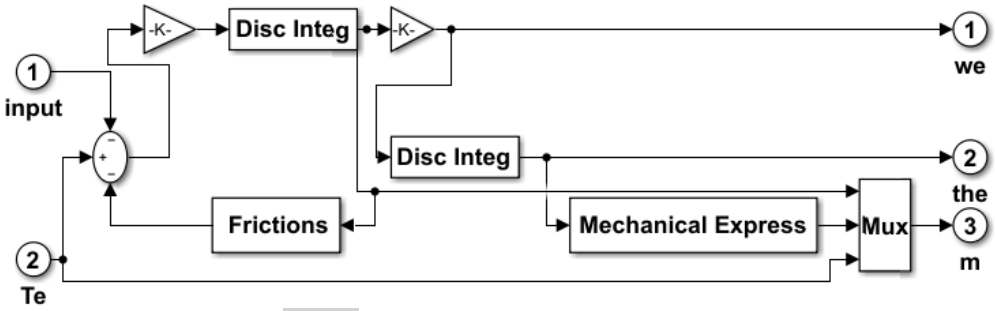

Fig. 4 Mechanical Part of the PMSM.

According to [12], the PMSM electrical dynamic equations mention both the Park transformation, which preserves the current and voltage modulus. The synchronous rotor frame with the d-axis aligned to the rotor flow. The Park Transform block implements the transformation from an a-phase to a q-axis alignment, as shown in Eq. (11).

$$\begin{bmatrix} d \\ q \\ 0 \end{bmatrix} = \begin{bmatrix} \sin(\theta) & \sin\left(\theta - \frac{2\pi}{3}\right) & \sin\left(\theta + \frac{2\pi}{3}\right) \\ \cos(\theta) & \cos\left(\theta - \frac{2\pi}{3}\right) & \cos\left(\theta + \frac{2\pi}{3}\right) \\ \frac{1}{2} & \frac{1}{2} & \frac{1}{2} \end{bmatrix} \begin{bmatrix} a \\ b \\ c \end{bmatrix} \quad (11)$$

The high saturation level is considered with PMSMs to achieve the best performance at high speeds. When the machine is run in different ways, its inductance values change in a way that is nonlinear because the machine's reluctance may be altered by the magnitude and phase angle of the current, which can also alter the magnetic flux distributions and the saturation of magnetic materials in the motor [13].

3.SLIDING MODE CONTROL TECHNIQUE

The SMC algorithm in Ref. [14] causes a chattering phenomenon in the controller's output. To mitigate this phenomenon, the discontinuous reaching law is replaced with the continuous reaching law. The position tracking error is defined by Eq. (12):

$$e = \theta - \theta_{ref} \quad (12)$$

where θ_{ref} and θ denote both the actual displacement and the reference position, respectively. Calculating the derivative of Eq. (12), the error is calculated in Eq. (13):

$$e' = \omega - \theta'_{ref} \quad (13)$$

The sliding surface of the system is designed as in Eq. (14):

$$s = e + \delta(e')^{mn} \quad (14)$$

where $0 < \delta < 1$, m and n are positive odd integers with $n < m < 2n$.

The SMC reaching law of the system is designed as in Eq. (15):

$$s' = -k|s + |s|^{\alpha} tanh\left(\frac{s}{\delta}\right) \quad (15)$$

The $tanh$ is a continuous function used instead of the sign discontinuity function to reduce the oscillations around the sliding surface, as shown in Fig. 5.

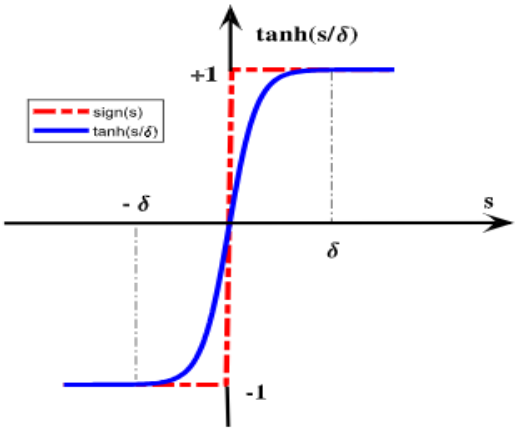

Fig. 5 Sign and $tanh$ functions.

Figure 5 shows the response of the sign and continuous tanh functions, δ>0, which are intermittently applied. According to Eqs. (11-15), the designed controller can be obtained as in Eq. (16):

$$i_q^* = a\left[\frac{(e')^{1-\lambda}}{\delta\lambda}(ks + k|s|^{\alpha}\tanh\left(\frac{s}{\delta}\right) + b\omega + \theta''_{ref} - \frac{e^{2-\lambda}}{\delta\lambda}\right] \quad (16)$$

where

$$\left[a = \frac{2j_o}{3n_p\psi_f}, b = \frac{B}{j_o}k\right]$$

and $k > 0$, and α is a positive odd integer with $\alpha < 1$.

where np is the pole pair, $J0$ is the system moment of inertia, B is the viscous friction coefficient, and ω is the motor angular velocity. The Simulink implementation for speed calculation is shown in Fig. 6 (a). The alpha-beta circuits are identical and can be implemented, as shown in Fig. 6 (b).

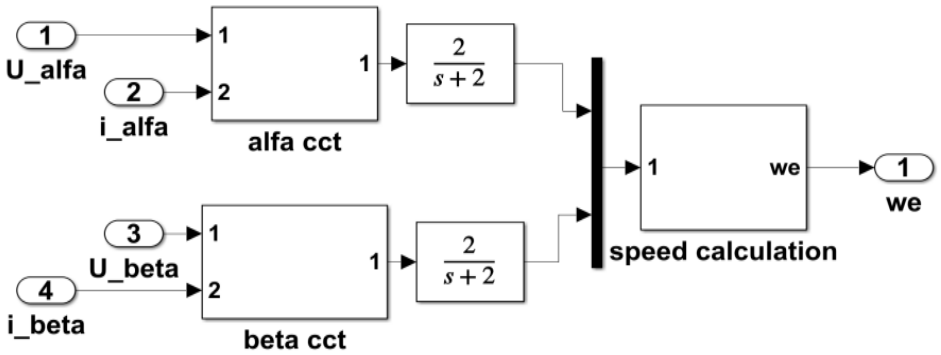

Fig. 6 (a) SMO Simulink Implementation.

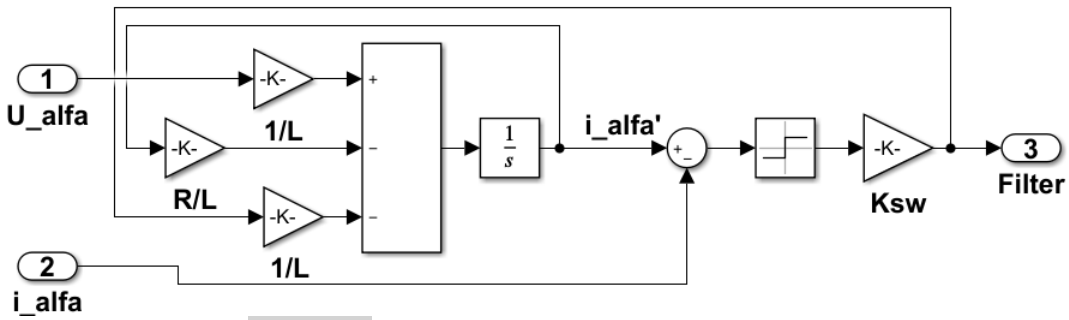

Fig. 6 (b) Alpha/beta Simulink Implementation.

The input of the first-order filter depends on the values of R and L, as presented in Table 1. A system with lower uncertainties requires a lower value of switching gain (Ksw). The SMC observer was suggested as a way to get accurate information about the rotor's position and lower the estimation error. As a result, the system responds quickly and follows the input signal without going off track [15], as seen in Fig. 7. Figure 8 illustrates the implementation of the complete PMSM controller using Simulink/MATLAB.

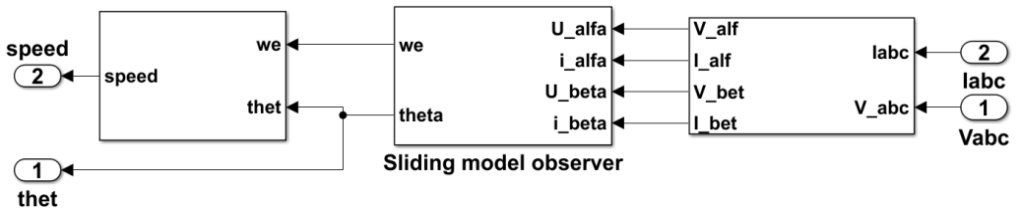

Fig. 7 SMO Correction Unit.

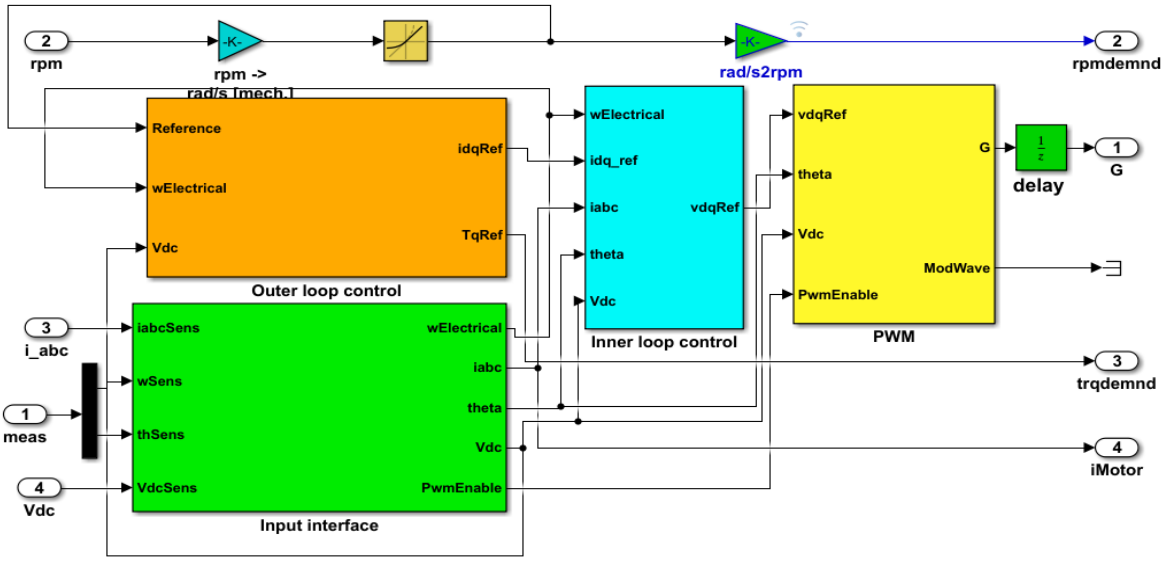

Fig. 8 PMSM Controller [16].

4.MULTILEVEL INVERTER

The primary varieties of multilevel inverters, together with the quantity of each type's components, are shown in Table 1 [17]. The inverter configuration is built like HiPako Module line-up, as shown in Fig. 9.

Table 1 Multilevel Inverter with the Required Number of Switches.

	Cascaded	Flying capacitor	Diode clamped
Main switching devices	(N-1)*2	(N-1)*2	(N-1)*2
Main diodes	(N-1)*2	(N-1)*2	(N-1)*2
Clamping diodes	0	0	(N-1)*(N-2)
DC bus capacitors	(N-1)/2	(N-1)	(N-1)
Balancing capacitors	0	[(N-1)*(N-2)]/2	0

Fig. 9 The HiPako Module Line-Up [18].

Using several standard half-bridge power modules, a 3-level NPC topology problem was developed. In the IGBT configuration, a high stray inductance is defined as an elevated in-series connection with a high switching di/dt ratio. The problem can be solved utilizing half-bridge IGBT modules [19]. Utilizing loss calculation blocks, three half-bridge IGBTs are used to execute the Phase-A leg. Compute and inject switching and conduction losses into a

thermal network. The three-phase, three-level inverter's possible output power as a function of switching frequency is shown in the simulation. The implemented inverter is shown in Fig. 10. The inverter control circuit is implemented in MATLAB/Simulink, as depicted in Fig. 11. A PI controller uses a current regulator to produce the required voltage reference for the PWM inverter generator based on the current reference d-axis and q-axis (Id and Iq). The PI controller inputs are both measured and reference current quantities (Id,Iq) to produce Vd and Vq. The oscillation in voltage across the switches is reduced to half when the induced gate-source voltage amplitude and current conduction are eliminated during the turning off of the complementary switch [20]. The SVPWM simulation, as shown in Fig. 12 (a), is playing a vital role in the industry. The complementary diode clamped switching is shown in Fig. 12 (b). The 3-phase state-to-pulses decoder firing pulses are shown in Table 3.

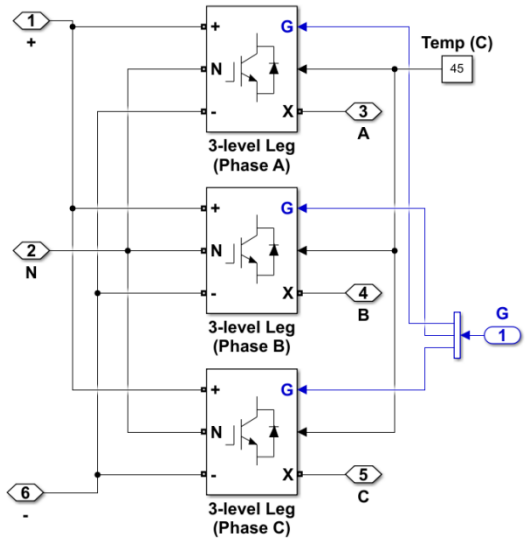

Fig. 10 Inverter Connection.

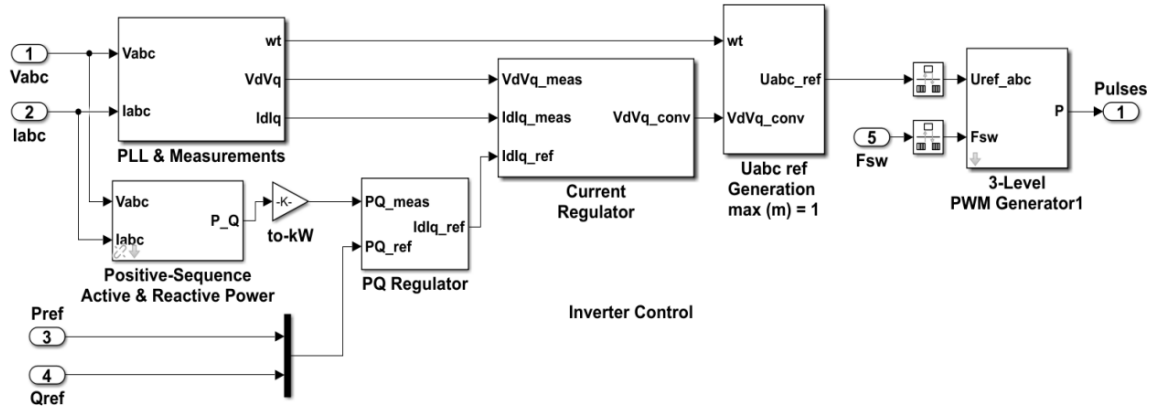

Fig. 11 Inverter Control Complete Circuit.

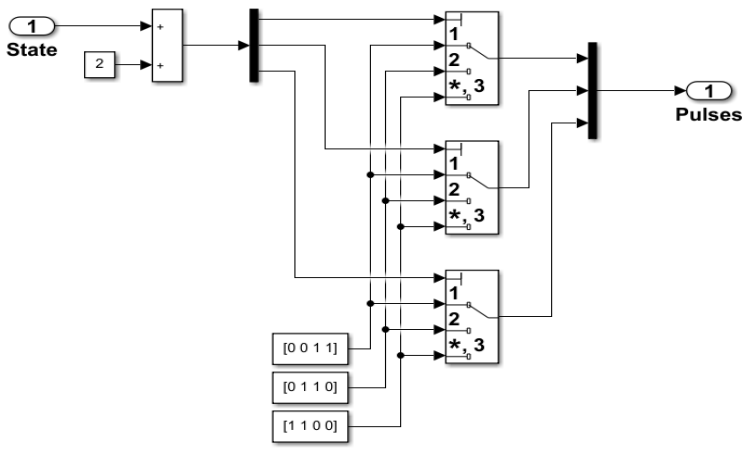

Fig. 12 (a) SVPWM Implementation.

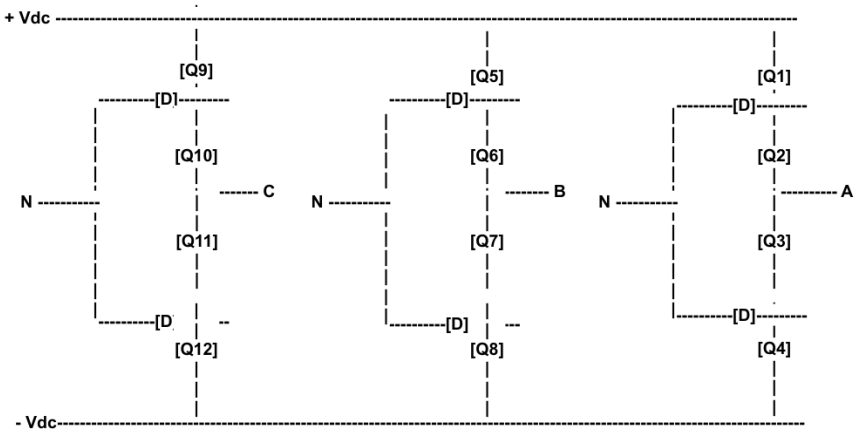

Fig. 12 (b) Complementary Diode Clamped Switching Arrangement.

Table 3 State/Pulse Configuration.

State	Q1	Q2	Q3	Q4
1	1	1	0	0
0	0	1	1	0
-1	0	0	1	1

Table 4 Pulse Pattern Configuration.

5: Q1 (phase B)	1: Q1 (phase A)	9: Q1 (phase C)
6: Q2 (phase B)	2: Q2 (phase A)	10: Q2 (phase C)
7: Q3 (phase B)	3: Q3 (phase A)	11: Q3 (phase C)
8: Q4 (phase B)	4: Q4 (phase A)	12: Q4 (phase C)

The modulation index is measured according to Eq. (17):

$$m_a = \frac{V_r}{V_c} \qquad (17)$$

where Vr is the maximum amplitude of the reference voltage signal, and Vc is the maximum amplitude of the carrier wave. The frequency modulation index (mf) is measured in Eq. (18):

$$m_f = \frac{f_c}{f_r} \qquad (18)$$

Where fc is the carrier frequency, *and* fr is the reference frequency.

5.WAVELET-BASED FEATURE EXTRACTION

The wavelet transform (WT) can extract local signal characteristics in the time-frequency domain [21]. In practice, Daubechies wavelets (db) allow for precise temporal and spatial analysis of dynamic waves in elastic materials. This method helps explain how elastic solids react to changing dynamic conditions. Adding the db to the finite wavelet domain method may have made transient dynamic waves in elastic solids more analyzable and robust [22]. Figure 13 shows a 6-level db10 wavelet.

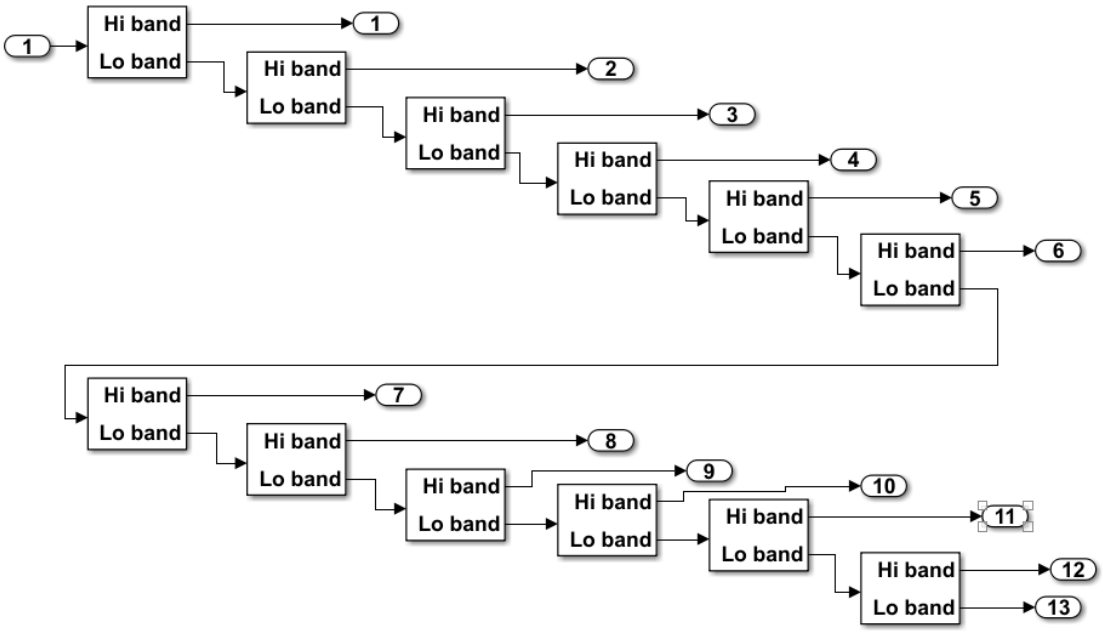

Fig. 13 Wavelet db10 with 6 Levels.

The continuous-time wavelet transform (CWT), which offers an affine-invariant time-frequency representation, is used in the majority of data analysis applications. The most popular variant, however, is the discrete wavelet transform (DWT), which is distinguished by its exceptional signal compaction features across a wide range of real-world signal classes and computing efficiency. Furthermore, since the DWT depends on up- and down-sampling methods in addition to flawless reconstruction filter banks, its implementation is simple. [23-24]. The discretized mother wavelet function can be defined as:

$$\psi_{m,n}(t) = a_0^{-\frac{m}{2}} \psi\left(\frac{t - nb_0 a_0^m}{a_0^m}\right) \quad (19)$$

And the corresponding DWT can be defined as [25-26]:

$$DWT_\psi x(m,n) = \int_{-\infty}^{\infty} \left(x(t)\psi^*_{m,n}(t)dt\right) \quad (20)$$

where $a0$ and $b0$ are fixed constants with $a0 > 1$ *and* $b0 > 0$, $m, n \in N$, and N is the set of positive integers. The wavelet decomposition levels are performed according to the criteria in Eq. (21):

$$Wdecomp = \frac{log(fs/f)}{log(2)} \pm 1 \quad (21)$$

where fs is the sampling frequency (10 kHz), and f is the source frequency.

Many comparative studies address the gap in highly advanced applications using nonlinear control or combined WT and SMC, such as [27-28]. The sensors' variation angle was estimated and shown in Fig. 14.

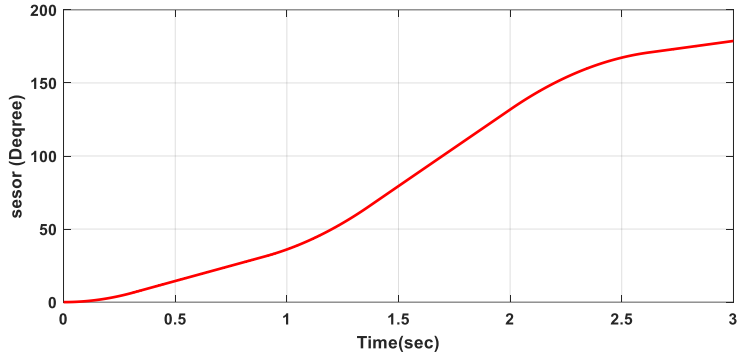

Fig. 14 Sensors Variation Angle.

Figure 14 shows that the nominal gain was selected as the least gain to force the system to converge. The convergence time (T) increased by values of $|\lambda x|$ when approaching the limit of stability of 180° to ensure the characteristic equation of the system:

$$1 + G(s)H(s) = 0 \quad (22)$$

In polar:

$$|G(s)H(s)| = 1, < 180 \quad (23)$$

The residual WT of the stator current is shown in Fig. 15. The original details coefficient of the current waveform is shown in Fig. 16. Figure 17 shows the wavelet details at level 5 of the PMSM motor current, as well as Simulink's implementation of the proposed diagnosis method. The switching frequency and modulation index were set in this algorithm to 10000 kHz and 0.85, respectively.

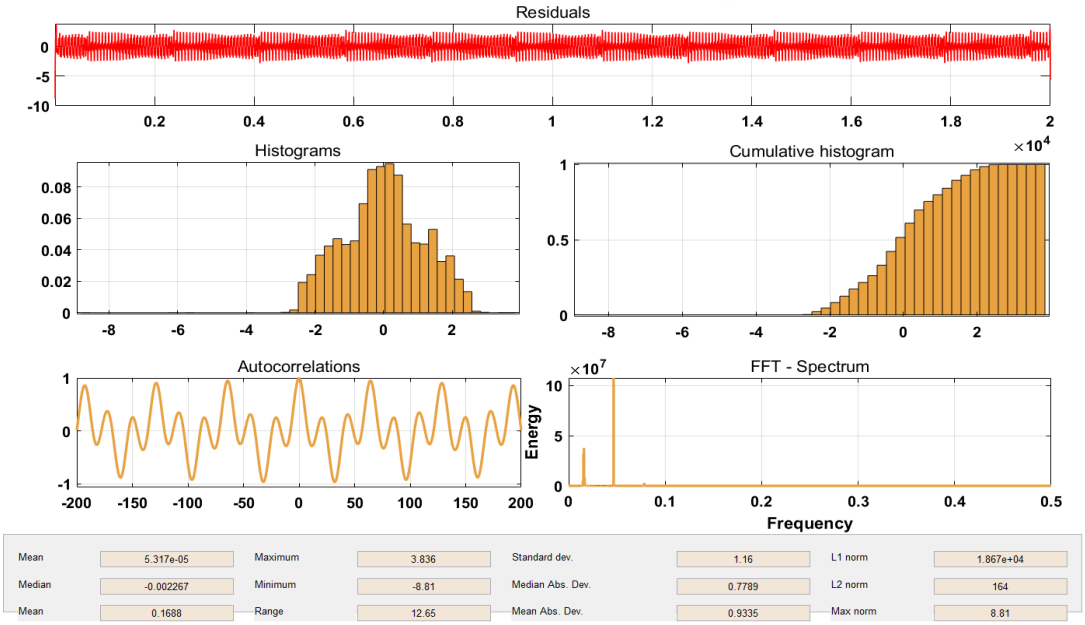

Fig. 15 Residuals of 1D Demising of db10 at level 5.

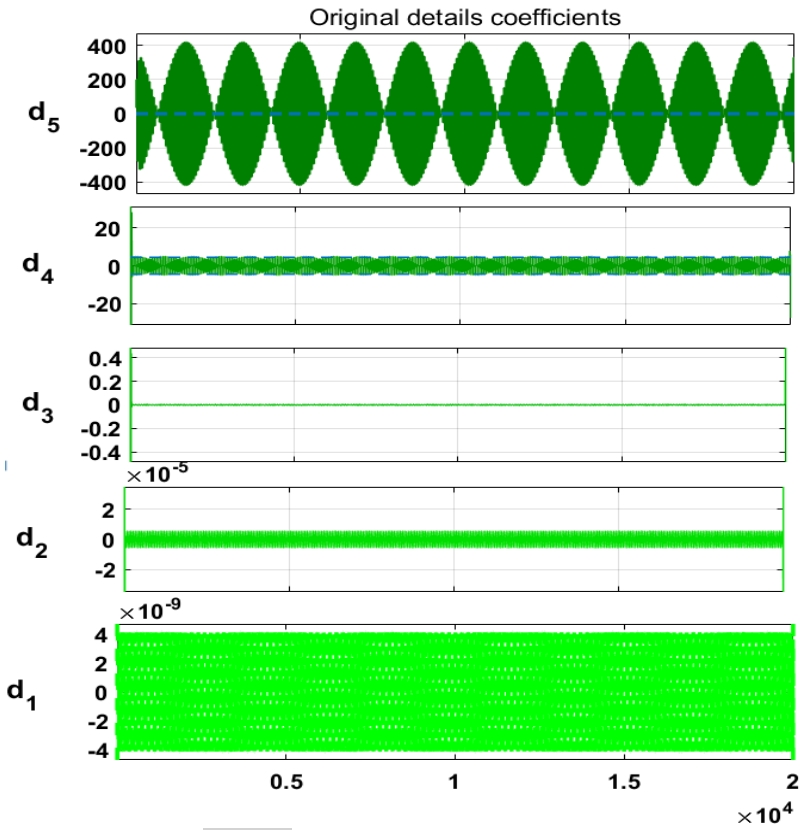

Fig. 16 Original Details Coefficients.

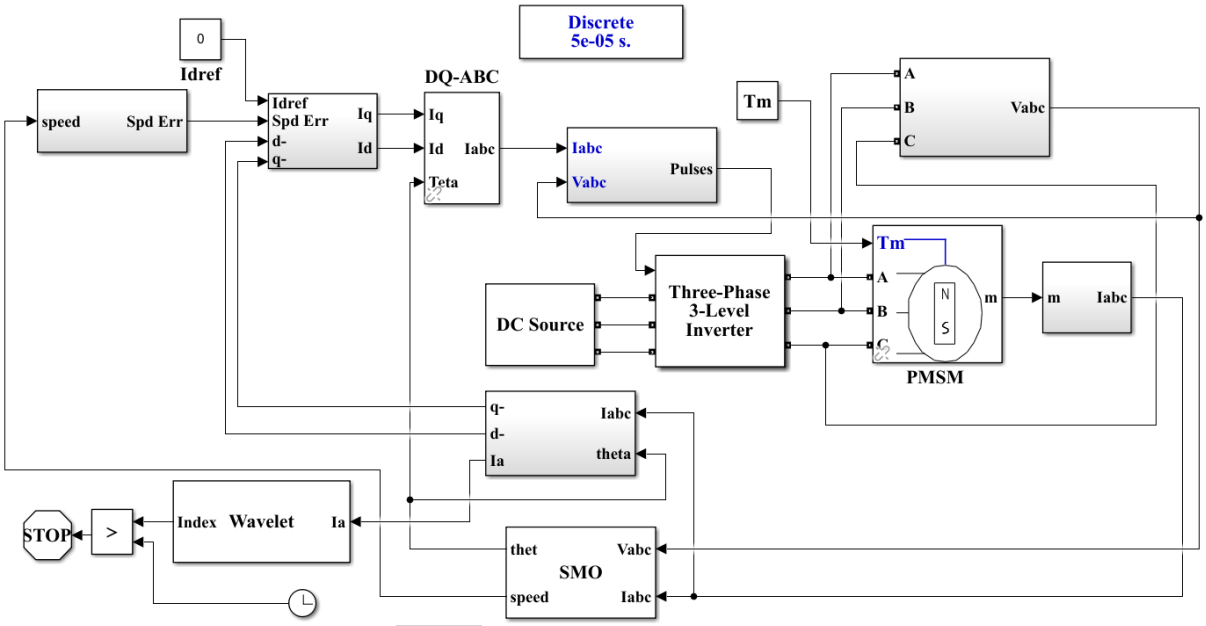

Fig. 17 Simulink Proposed Circuit.

6.CONTROL SYSTEM SIMULATION RESULTS

The software implementation of the suggested approach uses a wavelet toolkit and MATLAB/Simulink software to create a simulation drive control system for an electric machine. The validity and accuracy of the system were verified using the Simulink model, including the diode-clamp inverter and vector control. The simulation was conducted with a sampling period of 5e-5 sec and ideal switching devices of 0.85 Wb flux reference. Figure 18 displays the corresponding torque. For a large-scale operation, the estimated torque was close to the actual torque, as shown in Fig. 18. When the system worked properly, the error became small; hence, the PMSM operated smoothly. The power dissipated waveform is shown in Fig. 19. In rated condition, the 5 kW PMSM motor with a 500v-3LNPC inverter is shown in Fig. 20 (a and b).

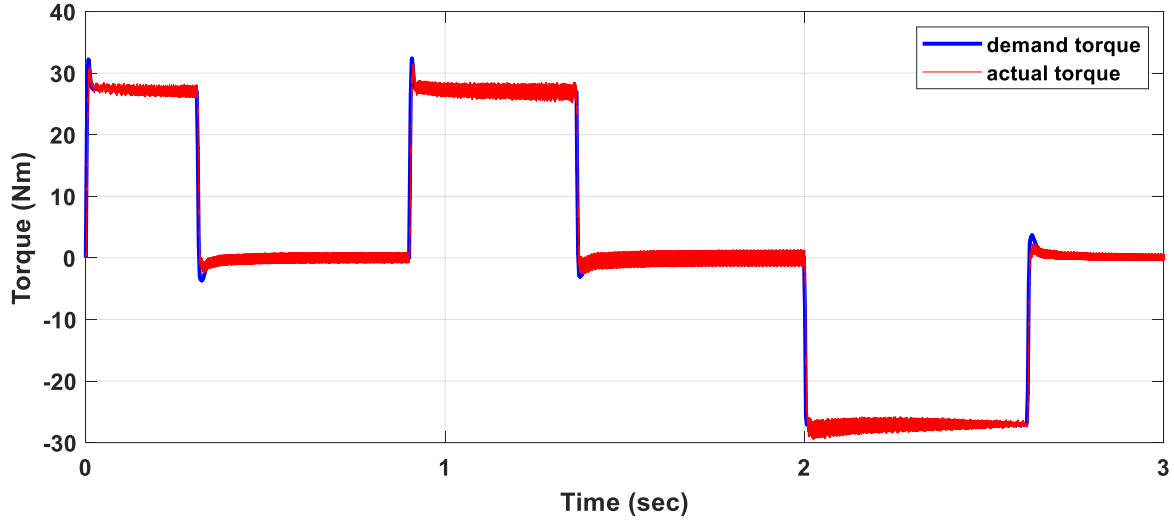

Fig. 18 PMSM Torque with its Reference.

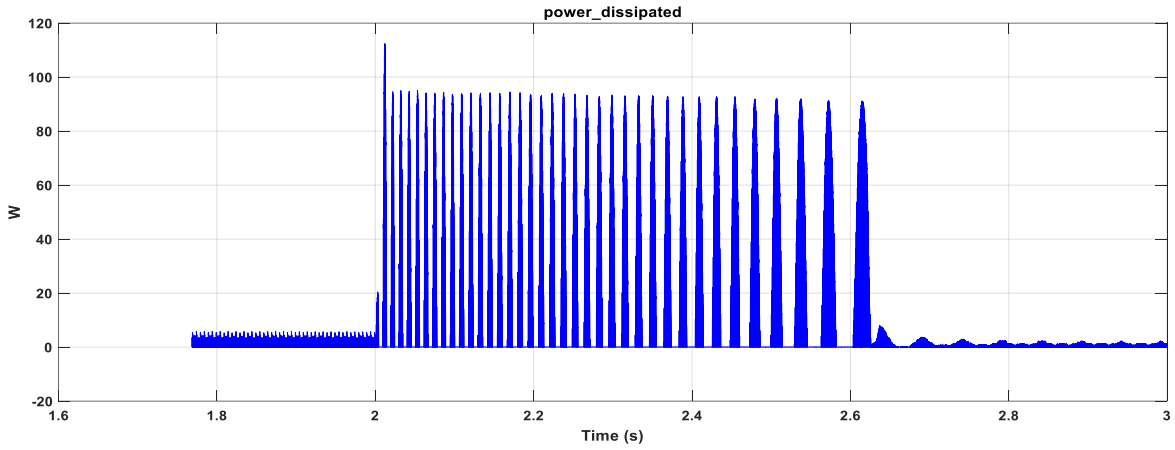

Fig. 19 Power Dissipated Waveform.

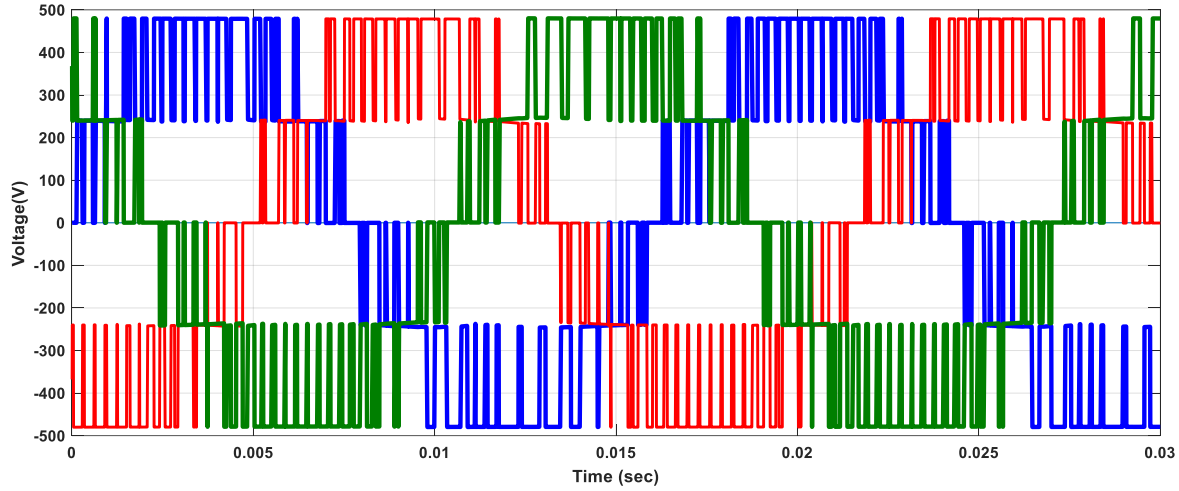

Fig. 20 (a) Diode-Clamped Inverter Voltage.

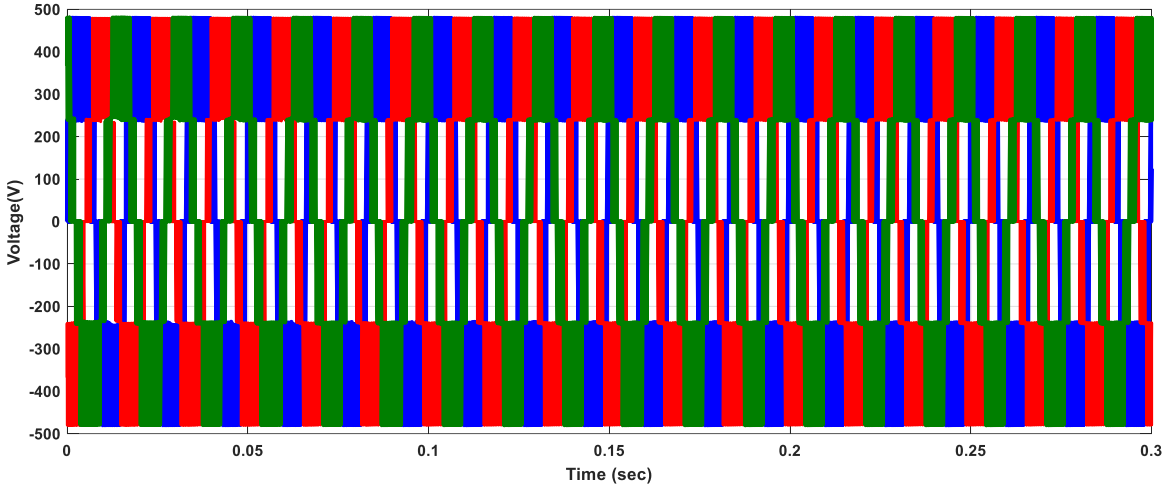

Fig. 20 (b) Diode-Clamped Inverter Voltage.

Figure 21 shows the speed command and tracking of the PMSM motor in various situations. When the speed command changed from (0–400) RPM at 1 sec, these were completely coincident. The system then increased and settled to 1000 RPM at (1-2.5) sec, before reducing to 200 RPM after 2.5 sec. The total harmonic distortion (THD) was very small in this system to ensure better operation, as shown in Fig. 22. Figure 23 shows the current waveform during the input mechanical torque in many situations. The PMSM controller employed two PI current controllers in both the inner and outer control loops, resulting in stator currents less than 2.5% of the THD. Figure 24 displays the components of the *Idq* current responses with the rotor speed of 400 rpm and the magnitude of the d–q axes reference voltages. The current response obtained with the proposed method is smoothly varied with respect to the reference speed due to the optimality considered in the sliding mode control. The space vector pulse width modulation was used to control the multilevel inverter [29], as shown in Fig. 25.

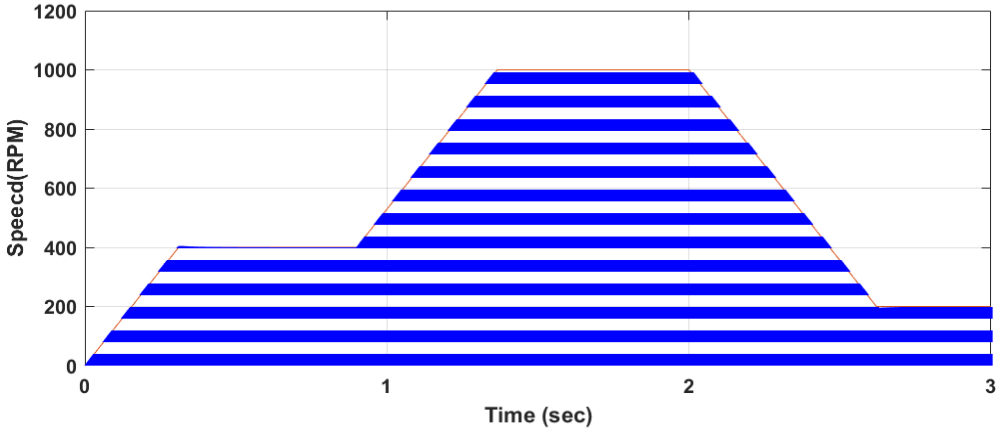

Fig. 21 PMSM Reference Speed.

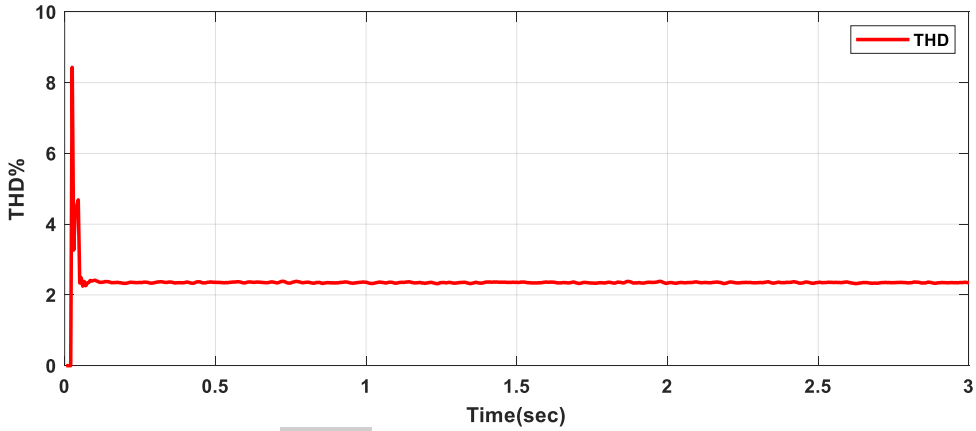

Fig. 22 Total Harmonic Distortion.

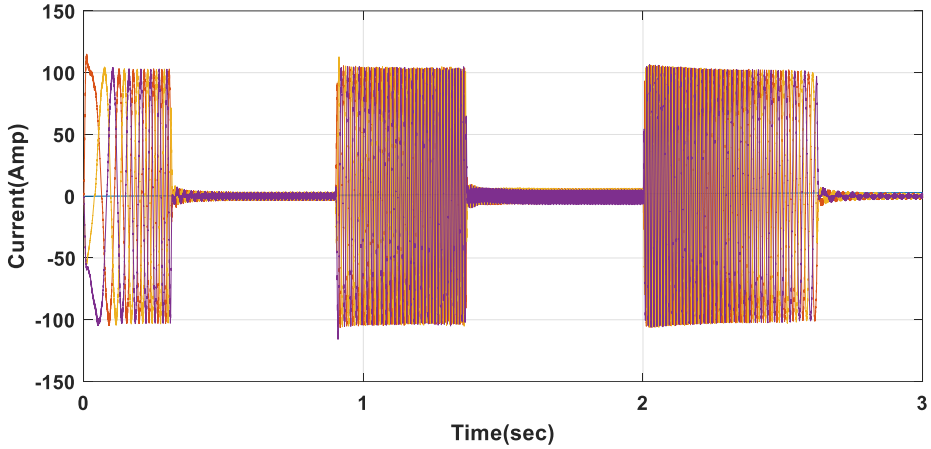

Fig. 23 The Stator Current Waveform Due to the Variable Reference Speed.

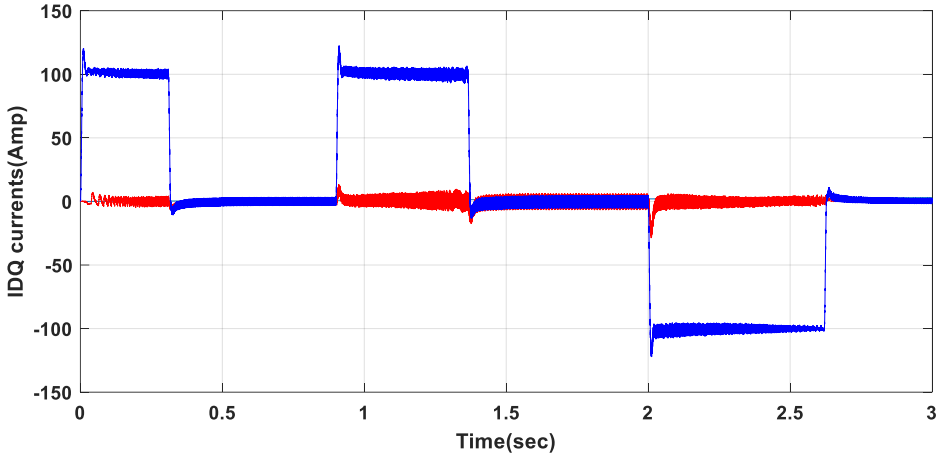

Fig. 24 PMSM *Idq* Current under the System Variation Parameter.

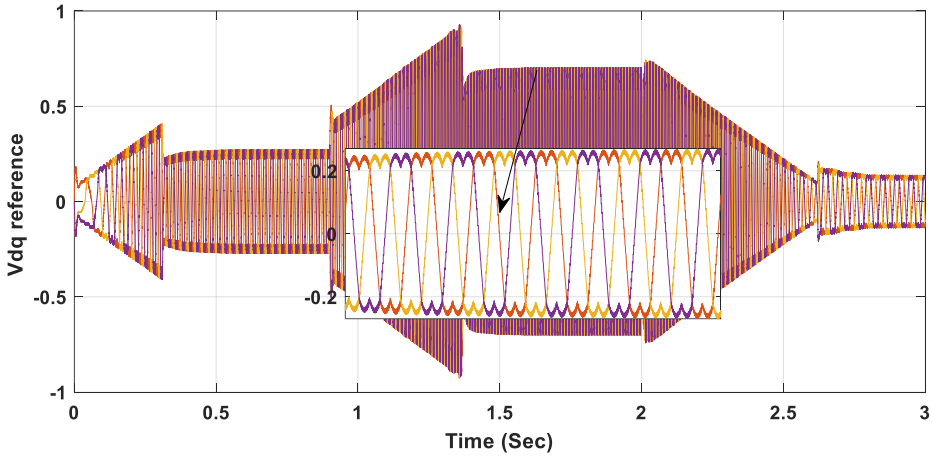

Fig. 25 SVPWM Effect of *Vdq* References.

7.CONCLUSIONS

In the present study, the simulation of the 3-phase with 3-level diode-clamped inverter and wavelet-based sliding mode control was performed using MATLAB/Simulink program. The PMSM power parameters were 5 kW, 220/380V, and 500 V at the DC-link. The SVPWM is a crucial modulation in the advanced control system of the machine drive to control the duty cycle of 0-99%. The db10 of WT was utilized to approximate the system uncertainties and yielded a minimum ksw to be used, eliminating the steady-state error. In addition, to ensure the system starts from the initial time without any delay, continuous tanh functions were used in the proposed control of the sliding surface. The simulation results showed that the proposed algorithm worked well for both the PMSM motor and machine drive operation.

REFERENCES

[1] Song Z, Xiao X, Yang J, Tao T, Mei X. **A Novel Sliding Mode Control with MRAS Inertia Identification for Permanent Magnet Synchronous**

Motors. *Measurement and Control* 2024; **57**(3): 240-250.

[2] Quang Tho Tran. **An Application of Neural Network-Based Sliding Mode Control for Multilevel Inverters**. *Engineering, Technology & Applied Science Research* 2024; **14**(1): 12530-12535.

[3] Hi Hong Huong Ngo, Minh-Tam Nguyen, Vinh-Quan Nguyen. **An Improved Control Method for Direct Torque Control Based on Sliding Mode Control**. *TJE Journal* 2024; **19**(s102): 53-65.

[4] N.T.H. Huong. **Three-Phase Asynchronous Motor Control by Sliding Mode Control**. Master's Thesis, Ho Chi Minh City University of Technical Education; 2019.

[5] Ukashatu Abubakar, Saad Mekhilef, Khalaf S. Gaeid, Hazlie Mokhlis, Yousif Al Mashhadany. **Induction Motor Fault Detection Based on Multi-Sensory Control and Wavelet Analysis**. *IET Electric Power Applications* 2020; **14**(11): 2051-2061.

[6] Xie Q, et al. **Method for Flux Linkage Optimization of Permanent Magnet Synchronous Motor Based on Nonlinear Dynamic Analysis**. *Nonlinear Dynamics* 2019; **97**(4): 2067–2089.

[7] Qu L, Qiao W, Qu L. **An Extended State Observer Based Sliding Mode Speed Control for Permanent Magnet Synchronous Motors**. *IEEE Journal of Emerging and Selected Topics in Power Electronics* 2021; **9**(2): 1605–1613.

[8] Shanthi R, Kalyani S, Devie P M. **Design and Performance Analysis of Adaptive Neuro-Fuzzy Controller for Speed Control of Permanent Magnet Synchronous Motor Drive**. *Soft Computing* 2020; **25**(2): 1519–1533.

[9] Taha A. Hussein, Ibrahim I. Sheet. **Implementation of Selective Harmonics Elimination for Single Phase Inverter Using Arduino and Simulink MATLAB Model**. *Tikrit Journal of Engineering Sciences* 2020; **27**(3): 31-37.

[10] Xu Y P, Zhong Y R, Yang H. **Research on Vector Control and Direct Torque Control for Permanent Magnet Synchronous Motors**. *Power Electronics* 2008; **42**(1): 60-62.

[11] Wen Jun Xu. **Permanent Magnet Synchronous Motor with Linear Quadratic Speed Controller**. *Energy Procedia* 2012; **14**: 364–369.

[12] C. Miguel Espinar, D. Heredero Peris, R. Villafafila Robles, D. Montesinos Miracle. **Review of Flux Weakening Algorithms to Extend the Speed Range in Electric Vehicle Applications with Permanent Magnet Synchronous Machines**. *IEEE Access* 2023; **11**: 22961-22981.

[13] L. Chédot, G. Friedrich. **A Cross Saturation Model for Interior Permanent Magnet Synchronous Machine. Application to a Starter Generator**. *39th IAS Annual Meeting* 2004: 64–70.

[14] Huacai Lu, Dongxue Yang, Zhongde Su. **Improved Sliding Mode Control for Permanent Magnet Synchronous Motor Servo System**. *IET Power Electronics* 2023; **6**(2): 169-179.

[15] Xia P. **Speed Adaptive Sliding Mode Control with an Extended State Observer for Permanent Magnet Synchronous Motor**. *Mathematical Problems in Engineering* 2018; **2018**: 6405923: 1-13.

[16] Khalaf S. Gaeid, Takialddin Al Smadi, Ukashatu Abubakar. **Double Control Strategy of PMSM Rotor Speed Based Traction Drive Using Resolver**. *Results in Control and Optimization* 2023; **13**: 100301.

[17] Khalaf S. Gaeid, Rami A. Maher, Ali J. Lazim. **Multilevel Inverter Fault Tolerant Control with Wavelet Index in Induction Motor**. *Journal of Electrical Engineering & Technology* 2019; **14**(3): 1179–1191.

[18] Raffael Schnell, Manager Application. **High Voltage Phase Leg Modules for Medium Voltage Drives and Inverters**. *Power Electronics Europe* 2010; **3**.

[19] Thomas Radke. **Smart Solutions for 1500Voc 3-Level Central PV Inverters**. *EE Power* 2020.

[20] Babaki, Mohammad Sadegh Golsorkhi, Nicklas Christensen, Mehdi Baharizadeh, Stefan Behrendt, Jesco Beyer, Thomas Ebel. **Parasitic Based Model for Characterizing False Turn on and Switching Based Voltage Oscillation in Hybrid T-Type Converter**. *Electronics* 2024; **13**: 1808.

[21] Yuxing Lin, Hongyi Zhang, Wanqing Wu, Xingen Gao, Fei Chao, Juqiang Lin. **Wavelet Transform and Deep Learning Based Obstructive Sleep Apnea Detection from Single-Lead ECG Signals**. *Physical and Engineering Sciences in Medicine* 2024; **47**: 119–133.

[22] Christos V. Nastos, Dimitris A. Saravanos. **Multiresolution Daubechies Finite Wavelet Domain Method for Transient Dynamic Wave Analysis in Elastic Solids**. *International Journal*

for Numerical Methods in Engineering 2021; **122**(23): 7078–7100.

[23] Halidou A, Mohamadou Y, Ari AAA, Zacko E. **Review of Wavelet Denoising Algorithms**. *Multimedia Tools and Applications* 2023; **82**: 41539–41569.

[24] Fu HW, Zhang Z, Yan XY, Wang XL, Zhao ZL. **Improved Wavelet Modulus Maximum Method for Distributed Optical Fiber Temperature Sensing**. *Optical Engineering* 2022; **61**: 116109.

[25] Fan L, Wang Y J, Zhang H X, Li C, Huang X Y, Zhang Q, Xin X J. **Quaternion Wavelet Transform and a Feedforward Neural Network-Aided Intelligent Distributed Optical Fiber Sensing System**. *Sensors* 2023; **23**: 3637.

[26] Khalaf S. Gaeid, Ayad Tariq Mahmood. **Review and Case Study on Control of Induction Motor Using High-Level Converter**. *Anbar Journal for Engineering Science* 2024; **15**(1): 41-53.

[27] Ameziane M, Slaoui K, Boumhidi I. **Adaptive Wavelet Network Sliding Mode Control for a Photovoltaic-Pumping System**. *Australian Journal of Electrical and Electronics Engineering* 2016; **13**(1): 24–31.

[28] Zahraoui Y, Zaihidee F M, Kermadi M, Mekhilef S, Mubin M, Tang J R, Zaihidee E M. **Fractional Order Sliding Mode Controller Based on Supervised Machine Learning Techniques for Speed Control of PMSM**. *Mathematics* 2023; **11**(6): 1457.

[29] Sajjad R. Hameed, Tahani H. AL-Mhana. **Cascaded H–Bridge Multilevel Inverter: Review of Topologies and Pulse Width Modulation**. *Tikrit Journal of Engineering Sciences* 2024; **31**(1): 138-151.